Biosensors and Bioelectronics 142 (2019) 111547

Contents lists available at ScienceDirect

Biosensors and Bioelectronics

journal homepage: www.elsevier.com/locate/bios

A smart hydrogel system for visual detection of glucose

Mingxin Wu[a], Yujie Zhang[a], Quan Liu[a], He Huang[a], Xin Wang[a], Zhekun Shi[a], Yinping Li[b], Sheng Liu[a], Longjian Xue[a,**], Yifeng Lei[a,*]

[a] School of Power and Mechanical Engineering & The Institute of Technological Science, Wuhan University, Wuhan, 430072, China
[b] School of Basic Medical Sciences, Wuhan University, Wuhan, 430071, China

ARTICLE INFO

Keywords:
Diabetes
Hydrogel
Glucose-responsive swelling
Glucose sensing

ABSTRACT

Glucose sensing is of vital importance due to the growing number of diabetes. In this study, we developed a visual detecting approach for glucose sensing based on a smart hydrogel system, by assembling of a photo-crosslinkable hydrogel and a pH-responsive nanogel, respectively. The hydrogel system showed fast response and high sensitivity to glucose in the physiological ranges, and enabled a visual detection of glucose both *in vitro* in glucose solutions and *in vivo* in diabetic mouse models. In normoglycemic state, the hydrogels showed large swelling, resulting in a large shape but with weak color or fluorescence intensity of the hydrogels. In hyperglycemic state, the hydrogels exhibited less swelling, resulting in a small shape but with strong color or fluorescence intensity of the hydrogels. Based on the observation of the size change and intensity change of the hydrogels, we can visual the glucose levels by either colorimetry or fluorescence imaging. This hydrogel system provides a novel means for visual detection of glucose. Our study broadens the current applications of hydrogels, extending their potentials in clinical diagnosis of diabetes or glucose-related analysis.

1. Introduction

In the body, glucose is primary energy source for most living organisms, and blood glucose level is a significant biomarker in many diseases, such as diabetes, obesity and cancers (Hay, 2016; Maric et al., 2019; Saltiel and Kahn, 2001). Among them, diabetes are one of the most challenging health problems worldwide in recent years (Cho et al., 2018), and an estimated 425 million adults around the world are effected by diabetes in 2017 (Cho et al., 2018). Typical characteristic of diabetes is high levels of blood glucose (hyperglycemia) in the body (Kitabchi et al., 2009), timely detection and control of blood glucose within the normoglycemic range are the major goal of diabetes treatment (Saltiel and Kahn, 2001).

Therefore, glucose sensing is of vital importance, and becomes a focus of interest for researchers, clinicians and patients (Maric et al., 2019; Yun et al., 2009). Although there are commercial instrument-based products for the fast detection of serum glucose, the requirement of electrical power and electronic read-out circuits increased both design complexity and detection cost. Extensive researches have been developed for quantitative and reliable glucose sensing. Most of the glucose sensing can be categorized into two types: optical methods and electrochemical methods (Heller and Feldman, 2008; Steiner et al., 2011; Wang, 2008; Xianyu and Jiang, 2014), where electrochemical approaches are still the most popular in clinical/home use.

The burgeoning nanomaterials and nanotechnology offer a great opportunity to facilitate glucose sensing based on optical or electrochemical methods. For example, gold nanorods and silver nanoparticles (Xianyu et al., 2013), MOF based-fluorescence platform (Cui et al., 2019), MWCNT-decorated polymeric nanoparticles (Xu et al., 2019), MoS_2 nanosheet (Lin et al., 2014), functionalized NiO nanoparticles (Liu et al., 2015), AIE-active bioprobe (Song et al., 2016), dual-emission hybrid of silica microbeads and CdTe quantum dots (Lu et al., 2016), nanofibrous guanosine-molecular hydrogel (Zhong et al., 2018), and GLUT1-rich cancer cell members (Kim et al., 2019) have been previously developed for detection of glucose. However, glucose sensors utilizing solid-state materials (for example, silica, CdTe, MoS_2 or NiO) are not fully compatible with biological systems for implantation *in vivo* (Nichols et al., 2013). Solid-state materials may cause infection and foreign body responses at an implanted site, resulting in inflammation and discomfort to patients (Vaddiraju et al., 2010).

Hydrogels have been extensively utilized in biomedical applications due to their excellent biocompatibility, tunable mechanical properties, and capability to incorporate functional groups for sensing (Hoffman, 2012). Hydrogels are very suitable for detecting different kind of

* Corresponding author.
** Corresponding author.
E-mail addresses: xuelongjian@whu.edu.cn (L. Xue), yifenglei@whu.edu.cn (Y. Lei).

https://doi.org/10.1016/j.bios.2019.111547
Received 4 July 2019; Received in revised form 25 July 2019; Accepted 27 July 2019
Available online 30 July 2019
0956-5663/

analytes and can be used in a wide filed of sensing applications (Doring et al., 2013). Hydrogels are sensitive to various environmental conditions depending on the nature of the functional groups, structure and composition (Culver et al., 2017; Koetting et al., 2015; Tokarev and Minko, 2009). Hydrogels are particularly suitable for designing the visual detection platform due to its negligible background color and fluorescence emission, as well as its large loading capacity and controllable shape (Hoffman, 2012).

Gelatin-methacrylamide (GelMA) hydrogels are biocompatible, and give wide ranging mechanical properties depending on several crosslinking parameters (Schuurman et al., 2013; Zhao et al., 2016). Polymer concentration, UV exposure time, and thermal gelation prior to UV exposure allow for the control of hydrogel stiffness and swelling properties (Schuurman et al., 2013).

Carboxymethyl cellulose (CMC) is widely used due to its good biocompatibility high biodegradability, easy availability and low cost (Liu et al., 2002; Wach et al., 2003). 2-hydroxyethyl acrylate (2-HEA) is also a biocompatible material, and often used as a grafting agent to improve the flexibility of CMC, in order to improve its mechanical properties (Tobing and Klein, 2001). Based on the grafting of 2-HEA into CMC, a pH-responsive hydrogel (CMC-pHEA) was produced, the CMC-pHEA hydrogel showed larger swelling ratio at high pH than at low pH (Park et al., 2018).

In the body, glucose reacts with oxygen to produce gluconic acid and hydrogen peroxide under the catalysis of glucose oxidase (GOx) (equation below). The produced gluconic acid reduces the pH and generates an acidic microenvironment. We supposed that we can utilize the pH changes during the glucose reaction, in order to induce different swelling of the hydrogels, thus achieve a visualization of glucose.

$$\text{Glucose} + O_2 + H_2O \xrightarrow{GO_X} \text{Gluconic acid} + H_2O_2$$

In this study, we develop a visual detecting approach for glucose sensing based on GelMA/CMC-pHEA hydrogel, which is composed of photo-crosslinkable GelMA hydrogel and pH-responsive CMC-pHEA nanogel, respectively. We investigated the changes of the size and intensity of the hydrogel system in response to glucose. The swelling of the hydrogel system in various glucose was quantitatively read out by an optical method, either colorimetry or fluorescence imaging, to realize a visualization of glucose both *in vitro* in glucose solutions and *in vivo* in diabetic mouse models.

2. Materials and methods

2.1. Materials

All chemicals were commercially available and used without further purification. Sodium carboxymethyl cellulose (CMC, average Mw 90,000), 2-hydroxyethyl acrylate (2-HEA), poly(ethylene glycol) diacrylate (PEGDA, Mw 700), potassium persulfate (KPS), sodium phosphate diabasic dodecahydrate ($Na_2HPO_4.12H_2O$), and D-(+)-glucose (reagent grade) were obtained from Sigma-Aldrich. Gelatin methacrylate (GelMA, EFL-GM-60), lithium phenyl-2,4,6-trimethylbenzoylphosphinate (LAP) and blue-violet light source (3W, 405 nm) were obtained from Suzhou Intelligent Manufacturing Research Institute, China. Red pigment was purchased from Marie's Water Colour, China. Glucose oxidase (GOx, 100 U mg^{-1}), fluorescein isothiocyanate (FITC, Ex = 495 nm, Em = 525 nm) and rhodamine 110 (R110, Ex = 498 nm, Em = 520 nm) were purchased from Aladdin, China. Phosphate-buffered saline (PBS, pH ~ 7.2) was obtained from HyClone. Ultrapure water (Milli-Q) with a resistivity of 18.2 M was used throughout the study.

2.2. Preparation of GelMA

GelMA powder was dissolved in water at a mass/volume percent of 10%. Photoinitiator LAP was dissolved in 10% GelMA solution at a mass/volume percent of 0.05–0.1% in the dark, in order to prevent the crosslinking of GelMA under natural light. The compounds were mixed with bath sonication at 37 °C for 5 min, and then dissolved in 37 °C water bath during 30 min. The mixed solution was crosslinked into hydrogel instantaneously (~1 s) under irradiation of blue-violet light (405 nm). Uncrosslinked GelMA solution can be stored at 4 °C in the dark. Before next use, the GelMA solution can warm in a water bath at 37 °C for 30 min, and became in solution for use.

2.3. Synthesis of CMC-pHEA

We prepared the pH-responsive CMC-pHEA hydrogel according to a previous reported method (Park et al., 2018). In brief, 50 mL of distilled water and CMC (5.56×10^{-6} mol) were added into a 250 mL round-bottomed flask, and the mixture was stirred at 75 °C and 400 rpm in a water bath until the CMC was dissolved. Then, N_2 gas was introduced into the flask for 20 min to reduce the oxygen in the dissolved CMC solution, then KPS (1.85×10^{-5} mol) was added and the mixture was reacted for 20 min. Next, 2-HEA (3.92×10^{-2} mol) was added to the solution. When the reaction mixture became milky white, the crosslinker PEGDA (0.32×10^{-3} mol) was added into the solution, and the reaction was continued for another 3 h. Thereafter, the solution was cooled at room temperature. The compound was dialyzed with distilled water for 5 days to remove the unreacted chemicals, the obtained product was labelled as CMC-pHEA. Subsequently, CMC-pHEA was lyophilized with a freeze dryer (GOLD SIM, USA). The freeze-dried foam was dissolved in PBS solution (50% wt) to form CMC-pHEA hydrogel. CMC-pHEA hydrogel was pH-responsive in various pH solutions (Fig. S1). Then, CMC-pHEA hydrogel was broken down into CMC-pHEA nanogels (diameter ~ 150 nm, Supplementary experiment, Fig. S2) for 30 min using an ultrasonic homogenizer (JY92-IIN, China).

2.4. Preparation of GelMA/CMC-pHEA hydrogels

We prepared GelMA/CMC-pHEA hydrogels using different volume ratios of GelMA to CMC-pHEA (Fig. 1). In brief, the above prepared GelMA solution and CMC-pHEA nanogel solution was mixed at varied volume ratios of 1:3, 1:2, 1:1, 2:1, 3:1 and 6:1, respectively (Fig. 1). The mixed solution was crosslinked under irradiation of blue-violet light (405 nm). The volume ratio of GelMA to CMC-pHEA nanogel at 3:1 was used to prepare the GelMA/CMC-pHEA hydrogel system in the subsequent study. We are able to prepare the hydrogel system in different shapes with various templates like bars, stars, and so on (Fig. S3).

2.5. pH responsiveness of GelMA/CMC-pHEA hydrogels

Star-shaped GelMA/CMC-pHEA hydrogels were prepared with 3D-printed star-shaped templates (Fig. S3). For better visualization of the changes of hydrogels, water-soluble red pigment (0.045 g mL^{-1}) was

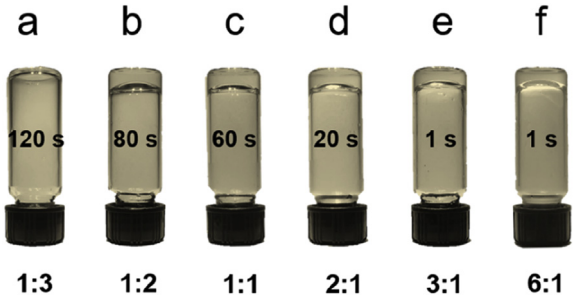

Fig. 1. Fabrication of GelMA/CMC-pHEA hydrogels. The volume ratio of GelMA to CMC-pHEA solution were (a) 1:3, (b) 1:2, (c) 1:1, (d) 2:1, (e) 3:1 and (f) 6:1.

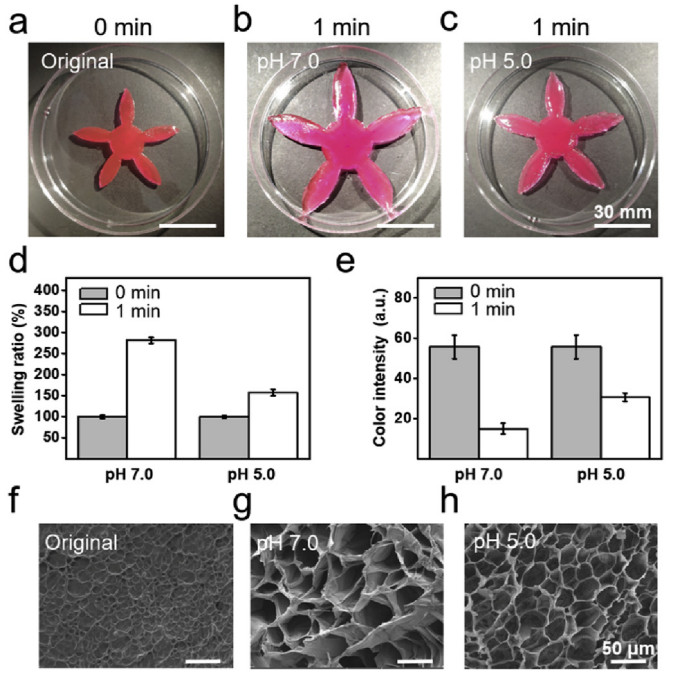

Fig. 2. Swelling of GelMA/CMC-pHEA hydrogels in various pH solution. (a) Star-shaped hydrogels before incubation in solution. The hydrogels were pre-loaded with red pigment. (b) Hydrogels incubated in neutral solution for 1 min. (c) Hydrogels incubated in acidic solution for 1 min. (d) Swelling ratio, and (e) red color intensity of the hydrogels incubated in pH 7.0 and pH 5.0 for 1 min, respectively. (f–h) SEM images of the cross-section morphology of freeze-dried hydrogels in (a–c), respectively.

dissolved in the mixed solution before crosslinking by blue-violet light irradiation.

After crosslinking (Fig. 2a), the star-shaped hydrogels were immersed in neutral solution (pH 7.0) and in acidic solution (pH 5.0), respectively (Fig. 2b and c). The changes of the shape and red color intensity of the hydrogels were monitored by photographing over time (Fig. 2, Movie S1).

Supplementary data related to this article can be found at https://doi.org/10.1016/j.bios.2019.111547.

2.6. Glucose sensing of GelMA/CMC-pHEA hydrogels in vitro

Bar-shaped GelMA/CMC-pHEA hydrogels were prepared using 3D-printed bar-shaped templates (length × width × thickness = 10 × 1 × 0.5 mm) (Fig. S3). Prior to the crosslinking of the hydrogels, the mixed solution of GelMA and CMC-pHEA nanogel (at volume ratio of 3:1) were added with excessive GOx (3000 U g^{-1}), and red pigment (0.045 g mL^{-1}) or fluorescent dyes (R110 (27.3 μM), or FITC (25.7 μM)). Then the mixture was crosslinked by blue-violet light irradiation. Subsequently, the hydrogels were incubated in glucose solutions (0, 5.55, 11.11, 16.66 and 22.22 mM, respectively) (Fig. 3a). Prior to do this, we proved that an acidic microenvironment was generated in glucose solutions over incubation time (Supplementary experiment, Fig. S4).

For the hydrogels containing GOx and red pigment, the changes of the hydrogels were recorded over time by photographing of the hydrogels (Fig. 3). For the hydrogels containing GOx and fluorescent dyes (R110 or FITC), the changes of the hydrogels were monitored over time using fluorescence modality of an *in vivo* imaging system (Bruker, Xtreme BI), with filter setting as excitation at 480 nm and emission at 535 nm (Fig. 4, Fig. S5).

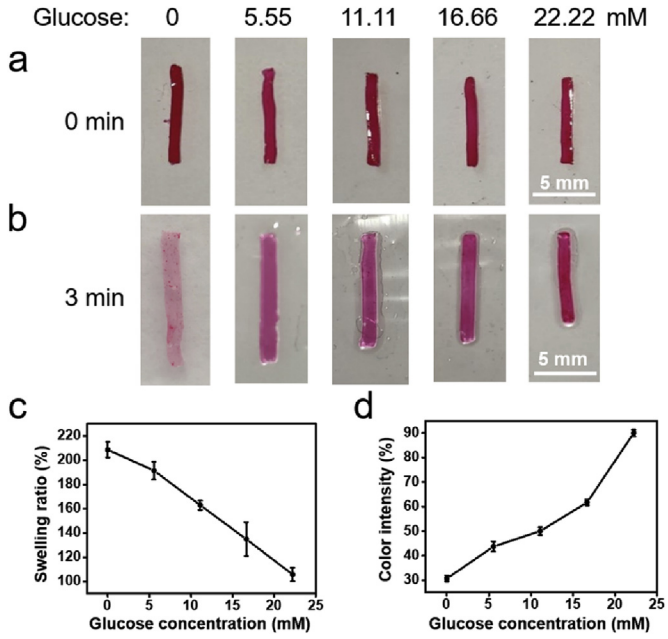

Fig. 3. *In vitro* glucose sensing by GelMA/CMC-pHEA hydrogels loaded with red pigment. (a) Images of bar-shaped hydrogels before incubation in glucose solutions. The hydrogels were pre-loaded with GOx and red pigment. (b) Images of hydrogels incubated in various glucose solutions for 3 min. (c) Swelling ratio, and (d) red color intensity of hydrogels incubated in various glucose solutions for 3 min, respectively.

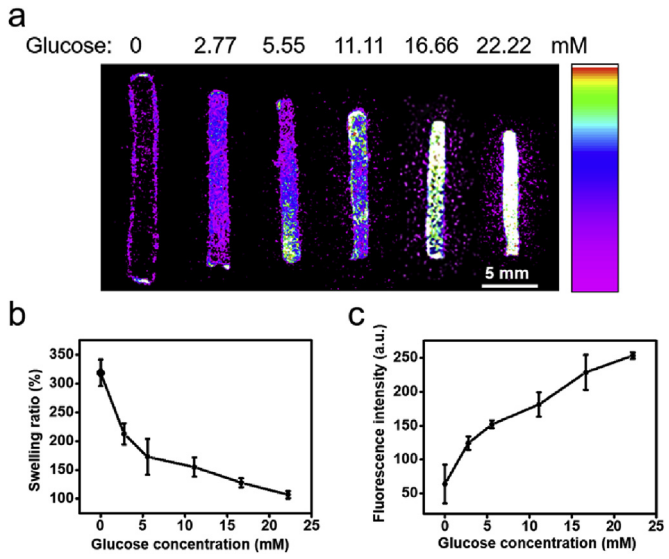

Fig. 4. *In vitro* glucose sensing by GelMA/CMC-pHEA hydrogels loaded with R110. (a) Fluorescence images of bar-shaped hydrogels incubated in various glucose solutions for 3 min. The hydrogels were pre-loaded with GOx and R110. (b) Swelling ratio, and (c) R110 fluorescence intensity of hydrogels incubated in various glucose solutions for 3 min, respectively.

2.7. Glucose sensing of GelMA/CMC-pHEA hydrogel in vivo

The Institutional Animal Care and Use Committee (IACUC) at Wuhan University approved all animal studies. Balb/c nude mice (8-week-old, male) were obtained from the Vital River Laboratory Animal Center (Beijing, China). Mice with various blood glucose levels were induced by intraperitoneal injection of streptozocin (STZ, Sigma-Aldrich) according to our empirical method (Zhang et al. 2019a, 2019b). By controlling the injection times and injection dosage of STZ, mice with different blood glucose levels (normoglycemia to

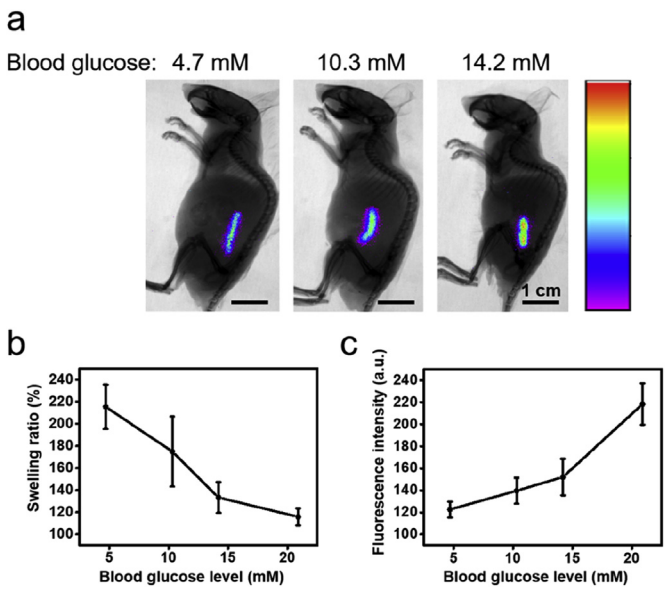

Fig. 5. *In vivo* glucose sensing by GelMA/CMC-pHEA hydrogels loaded with R110. (a) Fluorescence images of hydrogels implanted in mice with various blood glucose levels for 10 min. The hydrogels were pre-loaded with GOx and R110. (b) Swelling ratio, and (c) R110 fluorescence intensity of hydrogels implanted in mice for 10 min, respectively.

hyperglycemia) can be achieved. Blood from tail vein of mice (~5 μL) was collected for blood glucose detection with Sinocare GA-3 glucose monitor.

We injected a cylinder-shaped GelMA/CMC-pHEA hydrogel (length 10 mm, diameter 1 mm) into the subcutaneous dorsum of mice with help of a trocar (Fig. S6). Prior to the crosslinking of the hydrogel, the solution of GelMA and CMC-pHEA nanogel (at volume ratio of 3:1) were mixed with excessive GOx (3000 U g^{-1}) and fluorescent dyes (R110 (27.3 μM) or FITC (25.7 μM)). We filled the inner transparent tube of trocar with the mixed solution (Fig. S6a), and crosslinked the hydrogels under blue-violet light irradiation (Figs. S6b and c). Then we implanted the crosslinked hydrogel into the subcutaneous dorsum of the mice by pushing the inner tube of the trocar (Figs. S6b and d).

The changes of the hydrogels in mice were monitored using both fluorescence modality and X-ray modality of an *in vivo* imaging system (Bruker, Xtreme BI) (Fig. 5, Fig. S7), which records the fluorescence signal from the hydrogels in mice and the morphology of the mice, respectively.

2.8. Swelling ratio of the hydrogels

Surface area of the hydrogels at various time point were measured using ImageJ software (National Institutes of Health, NIH). The swelling ratio of the CMC-pHEA hydrogel or GelMA/CMC-pHEA hydrogels was calculated according to equation below:

$$\text{Swelling ratio (\%)} = S_t / S_0 \times 100\%$$

Where, S_t is the surface area of the swollen hydrogel at the time point t, and S_0 is the surface area of the original hydrogel before immersion into solution.

2.9. Intensity of the hydrogels

2.9.1. Red color intensity of the hydrogels

For the hydrogels loaded with red pigment, the photograph of the hydrogel was transformed into grayscale image (8-bit) using ImageJ software. Then the red color intensity from the red pigment of the hydrogels was analyzed with ImageJ software.

2.9.2. Fluorescence intensity of the hydrogels

Similarly, for the hydrogels loaded with fluorescent dyes (R110 or FITC), the Fluorescence images of the hydrogels were transformed into 8-bit images by ImageJ software, and the average fluorescence intensity of the hydrogels were analyzed by ImageJ software.

2.10. Scanning electronic microscopy

The three-dimensional network structure of freeze-dried GelMA/CMC-pHEA hydrogels was observed by scanning electronic microscopy (SEM, TESCAN MIRA3). The pore sizes of the hydrogels were calculated by ImageJ software.

3. Results

3.1. Preparation of CMC-pHEA nanogel

We synthesized CMC-pHEA hydrogel, a pH-responsive hydrogel, *via* radical polymerization based on CMC and 2-HEA (Park et al., 2018). The prepared CMC-pHEA hydrogel were sensible to pH changes, and the pH responsiveness of CMC-pHEA hydrogel was verified in various pH solutions (Fig. S1). With the pH of solution increasing from 5 to 7, the swelling of CMC-pHEA hydrogels progressively increased (Fig. S1). After 30 min incubation, the swelling ratio of CMC-pHEA hydrogel increased from 154% in pH 5.0 solution to 242% in pH 7.0 solution (Fig. S1). The pH-responsiveness of CMC-pHEA hydrogel was in accordance with the previous report, where CMC-pHEA hydrogel showed greater swelling ratio at pH 7.5 than at pH 5.5 (Park et al., 2018). This pH-responsiveness of CMC-pHEA hydrogel is due to the ionization of the carboxyl group (−COOH) of CMC and proton balance (Park et al., 2018). At pH 7.0, the carboxyl group of CMC ionized and the electrostatic repulsion existed between them, which extended the network further, and increased the swelling ratio of the hydrogel. At pH 5.0, most of the carboxyl group were protonated and strong hydrogen bonds between them caused dominant polymer-polymer interactions over polymer-water interaction, thus the swelling ratio of the hydrogel was limited.

However, the prepared CMC-pHEA hydrogel showed poor mechanical property, and it was hard to handle the CMC-pHEA hydrogel because of its fragility. Moreover, the swelling response of the CMC-pHEA hydrogel was slow, it took as long as 30 min to complete the swelling process (Fig. S1), which might be greatly reduced by decreasing the hydrogel dimensions. To solve these problems, we broken down the CMC-pHEA hydrogel into CMC-pHEA nanogels (diameter ~ 150 nm, Fig. S2), and then we introduced a second type of hydrogel, GelMA, as a skeleton to connect the CMC-pHEA nanogels.

3.2. Preparation of GelMA/CMC-pHEA hydrogel

We mixed the GelMA solution and CMC-pHEA nanogel solution in order to prepare the GelMA/CMC-pHEA hydrogels. On the one hand, GelMA ensures the ability of photo-crosslinking of the hydrogel system (Schuurman et al., 2013; Zhao et al., 2016), on the other hand, CMC-pHEA nanogels ensure the pH responsive ability of the hydrogel system (Park et al., 2018).

First, we evaluated the crosslinking behavior of GelMA/CMC-pHEA hydrogels with varied volume ratio of GelMA to CMC-pHEA (Fig. 1). When the ratio of GelMA to CMC-pHEA was small (1:3), it was difficult for the mixed solution to get crosslinked, the crosslinking time was longer than 120 s (Fig. 1a). When the mixing ratio increasing from 1:2 to 2:1, the crosslinking time of the hydrogels gradually decreased from 80 s to 20 s (Fig. 1b–d). As the mixing ratio increasing to 3:1, the crosslinking time of the hydrogels significantly shortened to 1 s (Fig. 1e). Meanwhile, the obtained hydrogels at 3:1 ratio had good mechanical properties and were convenient for handling for further operation. As the mixing ratio further increasing to 6:1, the crosslinking

time of the hydrogel remained at 1 s (Fig. 1f). However, the obtained hydrogel at 6:1 ratio was rigid and it was difficult for handling. Therefore, we used the mixing ratio at 3:1 to prepare the GelMA/CMC-pHEA hydrogels in the subsequent study without further indication. We can fabricate the hydrogel system in different shapes using different templates, such as bars, stars, and so on (Fig. S3).

3.3. pH responsiveness of GelMA/CMC-pHEA hydrogels

We evaluated the pH responsive ability of the GelMA/CMC-pHEA hydrogels in different pH solutions. We used the star-shaped hydrogels, which was pre-loaded with red pigment for better visualization.

In order to confirm the pH-responsive swelling behavior of the GelMA/CMC-pHEA hydrogels, we carried out a swelling study at pH 7.0 and pH 5.0, respectively (Fig. 2). The swelling of the GelMA/CMC-pHEA hydrogels was much faster than single CMC-pHEA hydrogel (Fig. S1, Fig. 2), which caused by the small size and large surface area of the CMC-pHEA nanogels (diameter ~ 150 nm, Fig. S2) in the hydrogel system. The swelling of the GelMA/CMC-pHEA hydrogels was completed in about 1 min, after that, the morphology of the hydrogel system no longer changed (Movie S1). After 1 min incubation, the swelling of the hydrogels at pH 7.0 was higher than at pH 5.0 (Fig. 2b and c). The hydrogels incubated at pH 7.0 had large swelling ratio (Fig. 2b, d), but the intensity of red pigment in the hydrogel was light (Fig. 2e). In contrast, the hydrogels placed at pH 5.0 had a relatively small swelling ratio (Fig. 2c and d), but with higher intensity of the red pigment in the hydrogel (Fig. 2e). These results indicate that the GelMA/CMC-pHEA hydrogel system is pH responsive. The pH responsive ability of the hydrogel system comes from the pH responsiveness of CMC-pHEA component.

Hydrogels generally swell when exposed to external solutions (Hoffman, 2012). Two important factors in the swelling kinetics and swelling ratio of a hydrogel are the pore size and pore structure (Hoffman, 2012). We confirmed the crosslinking network in the freezed-dried GelMA/CMC-pHEA hydrogels using SEM. Before immersion in solution, the hydrogels showed a porous structure, with an average pore size of 9.1 ± 3.6 μm (Fig. 2f). The hydrogels was classified as a super-porous hydrogel (Chen et al., 1999), in which pore diameters are greater than 1 μm. After immersion in neutral solution, the average pore size of the hydrogels increased to 38.1 ± 7.9 μm (Fig. 2g). After immersion in acidic solution, the pore size of the hydrogel less increased (Fig. 2h), with an average pore size of 25.3 ± 6.8 μm. The changes in pore sizes of the hydrogels (Fig. 2f–h) were in accordance with the swelling ratio of the hydrogels (Fig. 2a–c).

3.4. Visualization of glucose by GelMA/CMC-pHEA hydrogel in vitro

3.4.1. Colorimetry

In the body, glucose reacts with oxygen to produce gluconic acid and hydrogen peroxide under the catalysis of GOx (Fig. S4a). The produced gluconic acid results in an acidic microenvironment. We confirmed the pH changes in various glucose solutions containing GOx (Fig. S4b). Generally, the pH value of the glucose solutions decreased over incubation time (Fig. S4b). The higher the glucose concentration, the faster the pH of the solution decreased (Fig. S4b). For example, after 10 min incubation, the pH value in 22.22 mM glucose solution decreased to about 5.5, whereas the pH value in 5.55 mM glucose solution decreased to 6.6 (Fig. S4b). In solution without glucose, the pH did not change over incubation time (Fig. S4b).

We assume that we can employ these pH changes generated by various glucose solutions to induce different swelling of our hydrogel system (Fig. 2), in the aim to induce visualization of glucose concentrations. The glucose levels transformed into different pH values that enable direct observation by the changes of size and color intensity of the hydrogels (Fig. S4, Fig. 2). Thus, we investigated the glucose responsiveness of the GelMA/CMC-pHEA hydrogels in various glucose solutions (Fig. 3). Bar-shaped hydrogels were prepared using 3D-printed templates (Fig. 3a), which were pre-loaded with uniformly distributed GOx enzyme and red pigment in the hydrogels. To determine the sensitivity and linear range of hydrogels, we evaluated the glucose-sensing ability in physiological ranges (5.55, 11.11, 16.66, 22.22 mM, respectively).

The swelling of the GelMA/CMC-pHEA hydrogels in glucose solution was completed in about 3 min, after that, the morphology of the hydrogels no longer changed (Movie S2). After incubation in various glucose solutions, we observed a visible change in the size as well as the red color intensity of the hydrogels in glucose -dependent manner (Fig. 3b). In the absence of glucose, the swelling of hydrogels was the most significant, the relative surface area of the hydrogels was the largest, with the red color of the hydrogels became the lightest (Fig. 3b). In 22.22 mM glucose, the hydrogel showed the least swelling, with a relative smallest surface area, but the deepest red color of the hydrogels (Fig. 3b). The changes of the sizes and red color intensity of the hydrogels were linear to the glucose concentrations (Fig. 3c and d). With increasing glucose concentration from 0 to 22.22 mM, the swelling ratio of the hydrogels decreased from 210% to 110% (Fig. 3b and c), whereas the red color intensity of the hydrogels increased gradually from pink to deep red (Fig. 3b,d).

Supplementary data related to this article can be found at https://doi.org/10.1016/j.bios.2019.111547.

In low glucose concentration, the solution had a relatively high pH (Fig. S4b), thus the swelling of the hydrogels was large (Fig. 2), resulting in large size but weak color intensity of the hydrogels (Fig. 3). In contrast, in high glucose concentration, the solution exhibited a relatively low pH (Fig. S4b), thus the swelling of the hydrogels was limited (Fig. 2), resulting in a small shape but deep color intensity of the hydrogels (Fig. 3). Based on the *in vitro* results, we were able to visualize and deduce the glucose solution with unknown concentrations, according to the swelling ratio and color intensity of the hydrogel system (Fig. 3).

3.4.2. Fluorescence imaging

Besides loading red pigment into the GelMA/CMC-pHEA hydrogels for visualization of glucose with colorimetric method, we can also load fluorescent dyes into the hydrogels for fluorescent imaging of glucose solutions. We incorporated R110 dye into the hydrogels for glucose sensing (Fig. 4). We observed a similar tendency in changes of the hydrogels to that loaded with red pigment (Figs. 3 and 4). In low glucose concentration, the swelling of the hydrogels was large, thus the hydrogels exhibited a large shape but weak fluorescence intensity (Fig. 4). In contrast, in high glucose concentration, the swelling of the hydrogels was small, thus the hydrogels exhibited a small shape but strong fluorescence intensity (Fig. 4).

We have also loaded FITC dye into the hydrogels for glucose-sensing assay (Fig. S5). The swelling of the hydrogels showed a similar tendency as previous study (Fig. 4b, Fig. S5b), the swelling of the hydrogels decreased when increasing the glucose concentrations (Figs. S5a–b). However, the fluorescence intensity of the hydrogels showed an opposite tendency to the previous case (Fig. 4c, Fig. S5c), the FITC fluorescence intensity decreased when increasing the glucose concentrations (Figs. S5a and c). The abnormal changes in fluorescence intensity of the hydrogels attributed to the FITC dye incorporated in the hydrogels. FITC is a pH-sensitive fluorescent dye, and its fluorescence significantly quenches even disappears in acidic environments (Valeur and Leray, 2000). When increasing the glucose concentration, the pH of the solution gradually decreased (Fig. S4b), which induced significant fluorescence quenching of FITC (Valeur and Leray, 2000). Therefore, in high glucose concentration, even the swelling of the hydrogels was small, the fluorescence intensity of the hydrogels decreased (Figs. S5a and c). However, the FITC fluorescence quenching in the hydrogels in turn confirmed the generation of acidic microenvironment in high glucose concentration. The above results suggest that our hydrogel

systems are applicable for glucose sensing by incorporation of fluorescent dyes less sensitive to the pH fluctuations, such as R110 dye.

3.5. Visualization of glucose by GelMA/CMC-pHEA hydrogels in vivo

Subsequently, we evaluated the glucose sensing of the hydrogel system *in vivo* in diabetic mice, with different blood glucose levels ranging from normoglycemic to hyperglycemic states. Cylinder-shaped hydrogel was implanted into the subcutaneous dorsum of mice using a trocar (Fig. S6).

We investigated the glucose sensing of R110-loaded hydrogels in mice (Fig. 5). After 10 min implantation, the hydrogels in normoglycemic mice (blood glucose of 4.7 mM) exhibited a large shape but with weak fluorescence intensity (Fig. 5a). In contrast, the hydrogels in hyperglycemic mice (blood glucose of 14.2 mM) exhibited a small shape but with strong fluorescence intensity (Fig. 5a). From the statistical analysis, when the blood glucose levels of mice increasing from normoglycemic to hyperglycemic states, the swelling of the hydrogels in mice decreased (Fig. 5b), whereas the R110 fluorescence intensity of the hydrogel gradually increased (Fig. 5c). Both *in vivo* assay in diabetic mice and *in vitro* experiment in glucose solutions showed similar tendency (Figs. 4 and 5), when increasing the glucose levels, the swelling ratio of hydrogels decreased (Figs. 4b and 5b), whereas the R110 fluorescence intensity gradually increased (Figs. 4c and 5c). Therefore, we can also deduce the blood glucose levels in mice with unknown levels, based on the swelling ratio and R110 fluorescence intensity of the hydrogels implanted in mice.

We also investigated the glucose sensing of FITC-loaded hydrogels in mice (Fig. S7). The swelling of the FITC-loaded hydrogels *in vivo* showed the similar tendency as R110-loaded hydrogels *in vivo* (Fig. S7, Fig. 5), that the swelling of the hydrogels decreased when increasing the blood glucose levels in mice (Figs. S7a and b). However, the fluorescence intensity of the FITC-loaded hydrogels showed an opposite tendency to that of the R110-loaded hydrogels *in vivo* (Fig. S7, Fig. 5), that the FITC fluorescence intensity of the hydrogels decreased when increasing the blood glucose levels of mice (Figs. S7a and c). Similarly to the above case of FITC-loaded hydrogels *in vitro* (Fig. S5), the abnormal changes of FITC fluorescence intensity in hydrogels *in vivo* was due to the fluorescence quenching of FITC in acidic environments (Valeur and Leray, 2000). In the hyperglycemic mice, an acidic microenvironment was produced around the hydrogels in mice (Fig. S4), which resulted in significant fluorescence quenching of FITC (Valeur and Leray, 2000).

4. Discussion

Glucose sensing is of vital importance in many diseases such as diabetes, obesity, and cancers (Hay, 2016; Maric et al., 2019; Saltiel and Kahn, 2001). In the last few years, efforts are arisen to fabricate low cost, easy operation, and visually readable glucose sensors. Hydrogels offer great opportunity for glucose sensing owing to their excellent properties such as unique solid-liquid interface, easy processability, and their responsiveness to various environmental conditions (Culver et al., 2017; Doring et al., 2013; Hoffman, 2012; Koetting et al., 2015; Tokarev and Minko, 2009).

In this work, we developed a smart hydrogel-based sensor for visualization of glucose. The hydrogel system was composed of photocrosslinkable GelMA hydrogel and pH-sensitive CMC-pHEA nanogels, respectively. GelMA enabled easy formation and enhanced the mechanical properties of the hydrogel system (Fig. 1). Meanwhile, the use of CMC-pHEA nanogels (~150 nm, Fig. S2) greatly shortened the pH-responsive time of the hydrogels from 30 min to 1 min (Fig. S1, Fig. 2).

The mechanism of glucose sensing by the GelMA/CMC-pHEA hydrogel system is based on glucose-induced swelling of the hydrogels, in which combined the acidic microenvironment generated in glucose solutions (Fig. S4) and the pH-responsiveness of the hydrogel system (Fig. 2). The pH changes generated by various glucose solutions (Fig. S4) were able to induce different swelling of the hydrogels (Fig. 2). The readout of the swelling of the hydrogels in various glucose can be easily recognized by optical methods, either by colorimetric method (Fig. 3), or by fluorescence imaging (Figs. 4 and 5). The higher concentration of glucose, the smaller is the shape of the hydrogels, and the deeper is the color or fluorescence intensity of the hydrogels (Figs. 3–5).

To demonstrate the sensitivity of GelMA/CMC-pHEA hydrogels toward glucose concentrations *in vitro*, we performed a series of glucose solution assay within physiological range (Figs. 3 and 4). The results demonstrate that the hydrogel system can accurately measure the glucose levels *in vitro*. Inspired by these exciting *in vitro* results, we tested the application of the hydrogel system for the visual detection of the glucose *in vivo*. The sensitivity of the hydrogel toward glucose levels was confirmed in STZ-induced diabetic mice with various blood glucose levels (Fig. 5). From normoglycemic to hyperglycemic mice, we observed significant changes in size and fluorescence intensity of the hydrogel system (Fig. 5). Since the general range of blood glucose concentrations in healthy and diabetic subjects is about 3–8 mM and 9–20 mM, respectively (Kitabchi et al., 2009), thus, our hydrogel system is applicable for visualization of glucose in physiological ranges, from healthy to diabetic subjects.

The main advantages of this hydrogel-based glucose sensor over current technologies include low cost, simple fabrication, fast response, good sensitivity, biocompatibility, and convenient readout for the visual detection of glucose. Our findings demonstrate the use of hydrogels is a powerful tool for visualization of glucose levels in diabetes. Since glucose plays a key role in many human pathological conditions, we believe that this hydrogel system can be widely used for drug discovery and for monitoring the development of glucose-related diseases (Hay, 2016; Saltiel and Kahn, 2001).

Taken together, our hydrogel system revealed a visual detection of glucose both *in vitro* in glucose solutions and *in vivo* in diabetic mouse models. The hydrogel system gave fast and excellent response to glucose levels in physiologically relevant ranges. The visualization of glucose levels was achieved from the swollen size and color or fluorescence intensity of the hydrogels.

In the future, this hydrogel system can be integrated with photonic crystals (Chung et al., 2011; Ito et al., 2019), in order to construct a structural color hydrogel (Fu et al., 2018; Qin et al., 2018), which permits a more visible detection of glucose with naked-eye readout. Hydrogels containing glucose-responsive principles, such as phenylboronic acid (PBA) (Guo et al., 2015; Liu et al., 2018; Yetisen et al., 2017), can also be developed for reversible glucose visualization. Moreover, real-time glucose monitoring *in vivo* (Heo et al., 2011) can also be developed based on the use of smart hydrogels.

5. Conclusions

In summary, we have successfully developed a smart hydrogel system for visual detection of glucose. The hydrogel system shows fast response and high sensitivity to glucose in the physiological ranges both *in vitro* in glucose solution and *in vivo* in diabetic mice. We can visualize the glucose levels based on the size changes and color intensity changes of the hydrogels. This hydrogel system provides a novel means for visual detection of glucose. Our study broadens the current applications of hydrogels, extending their potentials in glucose-related analysis and clinical diagnosis of diseases.

Conflict of interest

All authors declare no conflicts of interest.

CRediT authorship contribution statement

Mingxin Wu: Data curation, Formal analysis, Writing - original

draft. **Yujie Zhang:** Data curation. **Quan Liu:** Methodology. **He Huang:** Methodology. **Xin Wang:** Methodology. **Zhekun Shi:** Methodology. **Yinping Li:** Methodology. **Sheng Liu:** Supervision. **Longjian Xue:** Supervision, Validation. **Yifeng Lei:** Conceptualization, Funding acquisition, Writing - review & editing.

Acknowledgements

The authors acknowledge the financial supports from National Key R&D Program of China (No. 2018YFB1105100), National Natural Science Foundation of China (NSFC, No. 81871484), the Fundamental Research Funds for the Central Universities, China (No. 2042018kf0235), Natural Science Foundation of Hubei Province, China (No. 2018CFB639), and Wuhan Morning Light Plan of Youth Science and Technology , China (No. 2017050304010306).

Appendix A. Supplementary data

Supplementary data to this article can be found online at https://doi.org/10.1016/j.bios.2019.111547.

References

Chen, J., Park, H., Park, K., 1999. J. Biomed. Mater. Res. 44, 53–62.
Cho, N.H., Shaw, J.E., Karuranga, S., Huang, Y., da Rocha Fernandes, J.D., Ohlrogge, A.W., Malanda, B., 2018. Diabetes Res. Clin. Pract. 138, 271–281.
Chung, W.J., Oh, J.W., Kwak, K., Lee, B.Y., Meyer, J., Wang, E., Hexemer, A., Lee, S.W., 2011. Nature 478, 364–368.
Cui, Y., Chen, F., Yin, X.-B., 2019. Biosens. Bioelectron. 135, 208–215.
Culver, H.R., Clegg, J.R., Peppas, N.A., 2017. Acc. Chem. Res. 50, 170–178.
Doring, A., Birnbaum, W., Kuckling, D., 2013. Chem. Soc. Rev. 42, 7391–7420.
Fu, F.F., Shang, L.R., Chen, Z.Y., Yu, Y.R., Zhao, Y.J., 2018. Sci. Robot. 3, eaar8580.
Guo, B., Pan, G., Guo, Q., Zhu, C., Cui, W., Li, B., Yang, H., 2015. Chem. Commun. 51, 644–647.
Hay, N., 2016. Nat. Rev. Cancer 16, 635–649.
Heller, A., Feldman, B., 2008. Chem. Rev. 108, 2482–2505.
Heo, Y.J., Shibata, H., Okitsu, T., Kawanishi, T., Takeuchi, S., 2011. Proc. Natl. Acad. Sci. U.S.A. 108, 13399–13403.
Hoffman, A.S., 2012. Adv. Drug Del. Rev. 64, 18–23.
Ito, M.M., Gibbons, A.H., Qin, D., Yamamoto, D., Jiang, H., Yamaguchi, D., Tanaka, K., Sivaniah, E., 2019. Nature 570, 363–367.
Kim, I., Kwon, D., Lee, D., Lee, G., Yoon, D.S., 2019. Biosens. Bioelectron. 135, 82–87.
Kitabchi, A.E., Umpierrez, G.E., Miles, J.M., Fisher, J.N., 2009. Diabetes Care 32, 1335–1343.
Koetting, M.C., Peters, J.T., Steichen, S.D., Peppas, N.A., 2015. Mater. Sci. Eng. R Rep. 93, 1–49.
Lin, T., Zhong, L., Guo, L., Fu, F., Chen, G., 2014. Nanoscale 6, 11856–11862.
Liu, L., Tian, X., Ma, Y., Duan, Y., Zhao, X., Pan, G., 2018. Angew. Chem. Int. Ed. 57, 7878–7882.
Liu, P., Zhai, M., Li, J., Peng, J., Wu, J., 2002. Radiat. Phys. Chem. 63, 525–528.
Liu, Q., Yang, Y., Li, H., Zhu, R., Shao, Q., Yang, S., Xu, J., 2015. Biosens. Bioelectron. 64, 147–153.
Lu, X., Wang, P., Wang, Y., Liu, C., Li, Z., 2016. Adv. Mater. Technol. 1, 1600024.
Maric, T., Mikhaylov, G., Khodakivskyi, P., Bazhin, A., Sinisi, R., Bonhoure, N., Yevtodiyenko, A., Jones, A., Muhunthan, V., Abdelhady, G., Shackelford, D., Goun, E., 2019. Nat. Methods 16, 526–532.
Nichols, S.P., Koh, A., Storm, W.L., Shin, J.H., Schoenfisch, M.H., 2013. Chem. Rev. 113, 2528–2549.
Park, S.H., Shin, H.S., Park, S.N., 2018. Carbohydr. Polym. 200, 341–352.
Qin, M., Sun, M., Bai, R., Mao, Y., Qian, X., Sikka, D., Zhao, Y., Qi, H.J., Suo, Z., He, X., 2018. Adv. Mater. 30, e1800468.
Saltiel, A.R., Kahn, C.R., 2001. Nature 414, 799–806.
Schuurman, W., Levett, P.A., Pot, M.W., van Weeren, P.R., Dhert, W.J.A., Hutmacher, D.W., Melchels, F.P.W., Klein, T.J., Malda, J., 2013. Macromol. Biosci. 13, 551–561.
Song, Z., Kwok, R.T., Ding, D., Nie, H., Lam, J.W., Liu, B., Tang, B.Z., 2016. Chem. Commun. 52, 10076–10079.
Steiner, M.S., Duerkop, A., Wolfbeis, O.S., 2011. Chem. Soc. Rev. 40, 4805–4839.
Tobing, S.D., Klein, A., 2001. J. Appl. Polym. Sci. 79, 2230–2244.
Tokarev, I., Minko, S., 2009. Soft Matter 5, 511–524.
Vaddiraju, S., Burgess, D.J., Tomazos, I., Jain, F.C., Papadimitrakopoulos, F., 2010. J. Diabetes Sci. Technol. 4, 1540–1562.
Valeur, B., Leray, I., 2000. Coord. Chem. Rev. 205, 3–40.
Wach, R.A., Mitomo, H., Nagasawa, N., Yoshii, F., 2003. Radiat. Phys. Chem. 68, 771–779.
Wang, J., 2008. Chem. Rev. 108, 814–825.
Xianyu, Y., Jiang, X., 2014. Curr. Opin. Chem. Eng. 4, 144–151.
Xianyu, Y., Sun, J., Li, Y., Tian, Y., Wang, Z., Jiang, X., 2013. Nanoscale 5, 6303–6306.
Xu, S., Zhang, Y., Zhu, Y., Wu, J., Li, K., Lin, G., Li, X., Liu, R., Liu, X., Wong, C.-P., 2019. Biosens. Bioelectron. 135, 153–159.
Yetisen, A.K., Jiang, N., Fallahi, A., Montelongo, Y., Ruiz-Esparza, G.U., Tamayol, A., Zhang, Y.S., Mahmood, I., Yang, S.A., Kim, K.S., Butt, H., Khademhosseini, A., Yun, S.H., 2017. Adv. Mater. 29, 1606380.
Yun, J.Y., Rago, C., Cheong, I., Pagliarini, R., Angenendt, P., Rajagopalan, H., Schmidt, K., Willson, J.K.V., Markowitz, S., Zhou, S.B., Diaz, L.A., Velculescu, V.E., Lengauer, C., Kinzler, K.W., Vogelstein, B., Papadopoulos, N., 2009. Science 325, 1555–1559.
Zhang, Y., Wu, M., Dai, W., Chen, M., Guo, Z., Wang, X., Tan, D., Shi, K., Xue, L., Liu, S., Lei, Y., 2019a. J. Nanobiotech. 17, 74.
Zhang, Y., Wu, M., Dai, W., Li, Y., Wang, X., Tan, D., Yang, Z., Liu, S., Xue, L., Lei, Y., 2019b. Nanoscale 11, 6471–6479.
Zhao, X., Lang, Q., Yildirimer, L., Lin, Z.Y., Cui, W., Annabi, N., Ng, K.W., Dokmeci, M.R., Ghaemmaghami, A.M., Khademhosseini, A., 2016. Adv. Healthc. Mater. 5, 108–118.
Zhong, R., Tang, Q., Wang, S., Zhang, H., Zhang, F., Xiao, M., Man, T., Qu, X., Li, L., Zhang, W., Pei, H., 2018. Adv. Mater. 30, e1706887.